Molecular Cell
Article

Structural Basis for Dimerization and Activity of Human PAPD1, a Noncanonical Poly(A) Polymerase

Yun Bai,[1] Sandeep K. Srivastava,[1] Jeong Ho Chang,[1] James L. Manley,[1] and Liang Tong[1,*]
[1]Department of Biological Sciences, Columbia University, New York, NY 10027, USA
*Correspondence: ltong@columbia.edu
DOI 10.1016/j.molcel.2011.01.013

SUMMARY

Poly(A) polymerases (PAPs) are found in most living organisms and have important roles in RNA function and metabolism. Here, we report the crystal structure of human PAPD1, a noncanonical PAP that can polyadenylate RNAs in the mitochondria (also known as mtPAP) and oligouridylate histone mRNAs (TUTase1). The overall structure of the palm and fingers domains is similar to that in the canonical PAPs. The active site is located at the interface between the two domains, with a large pocket that can accommodate the substrates. The structure reveals the presence of a previously unrecognized domain in the N-terminal region of PAPD1, with a backbone fold that is similar to that of RNP-type RNA binding domains. This domain (named the RL domain), together with a β-arm insertion in the palm domain, contributes to dimerization of PAPD1. Surprisingly, our mutagenesis and biochemical studies show that dimerization is required for the catalytic activity of PAPD1.

INTRODUCTION

Poly(A) polymerases (PAPs) are template-independent polymerases belonging to the nucleotidyl transferase superfamily (Aravind and Koonin, 1999). They are found in the nucleus, cytoplasm, and mitochondrion in eukaryotes as well as in bacteria, underscoring their functional importance. For example, almost all eukaryotic mRNAs, with the exception of histone mRNAs, are polyadenylated during maturation in the nucleus, which is important for their stability, transport to the cytoplasm, and translation (Colgan and Manley, 1997; Edmonds, 2002; Mandel et al., 2008; Proudfoot and O'Sullivan, 2002; Vinciguerra and Stutz, 2004; Zhao et al., 1999). A canonical PAP, PAPα in humans, catalyzes the polyadenylation of these mRNA precursors. The enzyme contains three domains: an N-terminal (palm) domain, a middle (fingers) domain, and a C-terminal (RNA binding) domain (Figure 1A) (Bard et al., 2000; Martin et al., 2000). The active site is located in the cleft between the palm domain and RNA binding domain (RBD) (Balbo and Bohm, 2007; Martin et al., 2004). Three highly conserved aspartic acid residues in the palm domain coordinate two divalent metal ions (Mg^{2+} or Mn^{2+}), which are essential for catalytic activity.

A class of noncanonical PAPs has also been identified, including seven such enzymes in humans (Kwak and Wickens, 2007; Martin and Keller, 2007; Mullen and Marzluff, 2008; Stevenson and Norbury, 2006). For example, Star-PAP is regulated by PIP_2 and targets select mRNAs in the nucleus (Mellman et al., 2008). GLD2 controls the length of poly(A) tails and regulates mRNA translation in the cytoplasm (Barnard et al., 2004). It also monoadenylates microRNA-122, leading to its stabilization (Katoh et al., 2009). Compared to the canonical PAPs, the noncanonical enzymes lack the RBD that follows directly after the fingers domain (Figure 1A), and it has been shown that GLD2 functions as a heterodimer with the RNA binding protein GLD3 in *C. elegans* (Kwak et al., 2004; Wang et al., 2002). Moreover, some of these noncanonical PAPs can add poly- or oligouridylates to their substrate RNAs and hence are also known as poly(U) polymerases (PUPs) or terminal uridylyltransferases (TUTases or TUTs) (Kwak and Wickens, 2007; Martin and Keller, 2007; Mullen and Marzluff, 2008; Rissland et al., 2007). This modification also has important roles for RNA function and stability. Star-PAP is required for uridylation of U6 snRNA (Trippe et al., 2006), and TUTase4 regulates the biogenesis of the let-7 microRNA (Heo et al., 2009).

PAPD1 (also known as mtPAP, TUTase1) is a noncanonical PAP that polyadenylates mitochondrial RNAs (Nagaike et al., 2005, 2008; Tomecki et al., 2004). This polyadenylation is required to complete the stop codon (UAA) for some mitochondrial mRNAs, and the poly(A) tail can probably regulate RNA stability as well. PAPD1 may also be important for the maturation of mitochondrial tRNAs. In contrast to GLD2, PAPD1 appears to be active on its own and does not require a separate RNA binding protein (Nagaike et al., 2005; Tomecki et al., 2004). Consistent with its role in the mitochondrion, PAPD1 is the only PAP in humans that contains a mitochondrial targeting sequence at the N terminus (residues 1–37) (Figure 1A). However, recent studies show that this enzyme, as well as TUTase3, can oligouridylate histone mRNAs for their degradation, suggesting that PAPD1 can also function as a TUTase in the cytoplasm (Mullen and Marzluff, 2008). Three single-nucleotide polymorphisms (SNPs) in PAPD1 have been linked to extreme obesity in cattle, one of which leads to a missense mutation, D39G (human PAPD1 numbering), just after the mitochondrial targeting sequence (Xiao et al., 2006).

While the canonical PAPs have been studied extensively at the structural level (Balbo and Bohm, 2007; Bard et al., 2000; Martin et al., 2000, 2004), no structural information is currently available

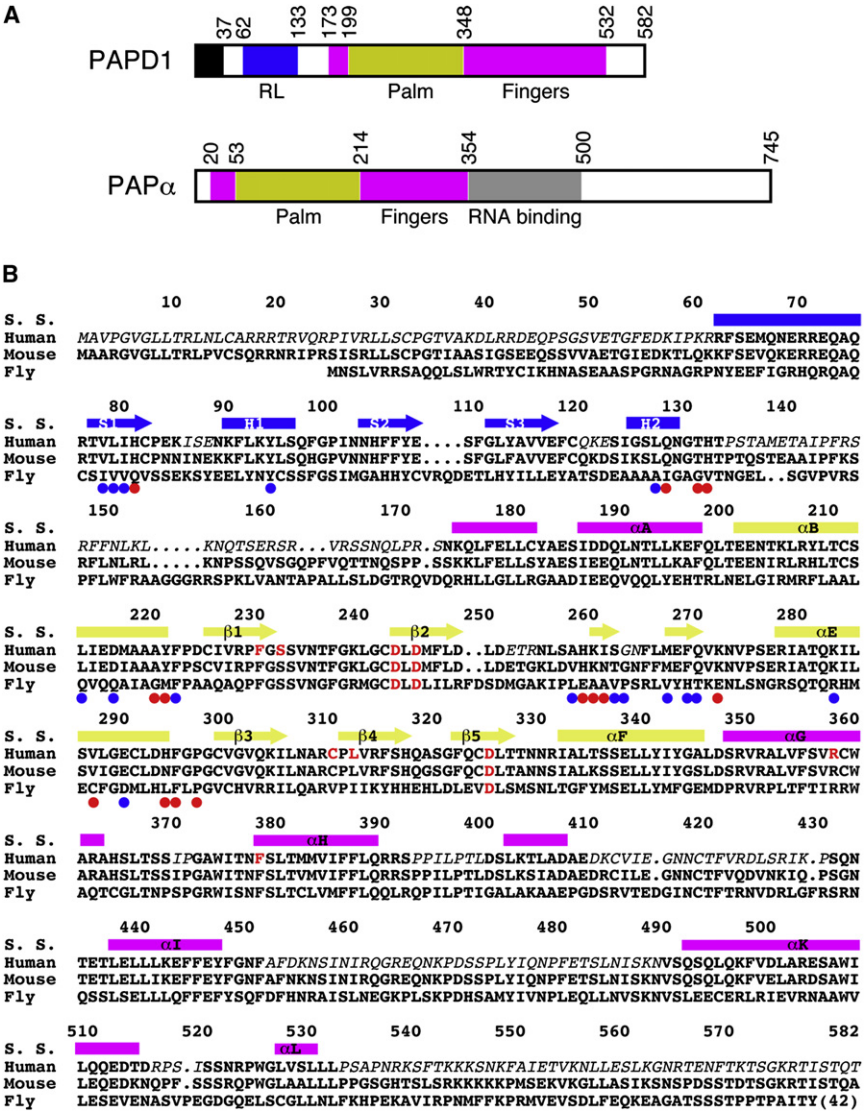

Figure 1. Sequence Conservation of PAPD1

(A) Schematic drawing of the domain organization of human PAPD1 and human PAPα. The various domains are labeled. The mitochondrial targeting sequence of PAPD1 is shown in black.

(B) Sequence alignment of human, murine and *Drosophila melanogaster* (Fly, CG11418) PAPD1. The secondary structure elements (S. S.) are labeled and colored according to the domains. Residues shown in red are in the active site. The colored dots highlight those residues with >50 Å^2 (red) or >20 Å^2 (blue) buried surface area in the dimer interface. Residues missing in the current structure of human PAPD1 are shown in italic. The sequence conservation between human and *Drosophila* PAPD1 for residues in the RL domain (25% identity) is lower compared to that for the palm and fingers domains (39% identity).

on the noncanonical PAPs. In addition, the sequence conservation between the two classes of enzymes is very low, around 10%–15%, despite their sharing the palm and fingers domains. We report here the crystal structure of a noncanonical PAP, human PAPD1. The structure defines the active site architecture of this enzyme and reveals a domain (RL domain) in the N-terminal region that contributes to its dimerization and has a backbone fold similar to RNP-type RBDs. Our mutagenesis and biochemical studies unexpectedly show that this dimerization is required for the catalytic activity of PAPD1.

RESULTS AND DISCUSSION

Structure Determination

We set out to identify a derivative of human PAPD1 that would produce crystals suitable for structural studies. After screening a large number of bacterial expression constructs containing various regions of PAPD1, we were able to obtain crystals for a derivative consisting of residues 44–538. However, the quality of these crystals was poor, and the best diffraction that was observed extended to about 3.5 Å resolution. We attempted to improve the diffraction quality by crystallizing the enzyme in complex with substrates (MgATP and/or oligonucleotides), and we mutated one of the conserved aspartic acid residues in the active site, D325A, equivalent to the D154A mutation in yeast PAP that was used to obtain a structure of that enzyme in complex with MgATP and oligo(A) (Balbo and Bohm, 2007). Interestingly, the mutant protein gave better-quality crystals than the wild-type enzyme, even though no nucleotides were bound, and we were able to determine its structure at 3.1 Å resolution by the selenomethionyl (SeMet) anomalous diffraction method (Table S1) (Hendrickson, 1991).

The refined structure has good agreement with the crystallographic data and the expected bond lengths, bond angles, and other geometric parameters (Table 1). The two molecules of PAPD1 in the asymmetric unit have similar overall structures, with rms distance of 0.45 Å between equivalent Cα atoms and similar temperature factor values (average *B* of 48 and 51 Å^2 for the two molecules). The somewhat higher R factor values are due to the many poorly ordered and disordered segments in the structure (Figure 1B). A few of the poorly ordered segments were modeled as poly-alanines (Figure 2A), due to insufficient electron density for the side chains, while the others were too discontinuous to be modeled. This would reduce the agreement between the structure model and the crystallographic data. This problem appears to be inherent to this protein, as we refined the model against a different reflection data set, collected on

Table 1. Summary of Crystallographic Information for Human PAPD1

Maximum resolution (Å)	3.1
Number of observations	73,621
R_{merge} (%)[a]	8.0 (28.9)
I/σI	9.0 (2.3)
Redundancy[b]	2.4 (2.0)
Resolution range used for refinement	30–3.1
Number of reflections[b]	28,985
Completeness (%)	92 (75)
R factor (%)	24.7 (32.6)
Free R factor (%)	32.8 (45.6)
rmsd in bond lengths (Å)	0.010
rmsd in bond angles (°)	1.4
Average temperature factor value (Å^2)	50
Number of protein atoms	5353
Number of solvent atoms	0

[a] The numbers in parentheses are for the highest-resolution shell. See also Table S1.
[b] The Friedel pairs are kept as separate reflections.

another crystal at a different synchrotron source, and obtained similar R factor values.

Overall Structure of PAPD1 Monomer

The structure of PAPD1 contains three domains: the canonical palm and fingers domains and a previously unrecognized domain in the N-terminal region (Figure 2A). Residues 199–347 form the palm domain, and the three catalytic aspartic acid residues (Asp243, Asp245, and Asp325, with the Asp325 residue mutated to alanine in the current structure) are located on the surface of the five-stranded β sheet in this domain (Figure 2A). A simulated annealing omit difference electron density map for this region is shown in Figure S1. The structure reveals that residues 253–273 form a β-hairpin that protrudes far away from the rest of the monomer. This structural feature is involved in dimerization of PAPD1 (see below), and we have named it the β-arm (Figure 2A).

Residues 173–198 and 348–532 form the fingers domain (Figure 2A). While the helices in this domain have good electron density, many of the connecting loops are poorly ordered or disordered in the crystal, even though their sequences are quite conserved among PAPD1 orthologs (Figure 1B). These disordered loops may be important for the function of PAPD1. Two of these loops were modeled as poly-alanines (Figure 2A), guided by the structure of yeast PAP (Balbo and Bohm, 2007). Residues 533–538 at the C terminus of this derivative were disordered in the crystal. In fact, secondary structure predictions suggest that the entire C-terminal segment of PAPD1, residues 533–582, is unstructured, and PAPD1 does not have an RBD directly following the fingers domain (Figure 1A).

The overall structure of the palm and fingers domains of PAPD1 is similar to that in the canonical PAPs, despite their low sequence conservation (Figure S2). Compared to the structure of yeast PAP in complex with MgATP and oligo(A) (Balbo and Bohm, 2007), the two domains are somewhat more open relative to each other, corresponding to a rotation of approximately 4° (Figure 2B). Substrate binding is expected to lead to a more closed conformation for PAPD1, as has been observed for yeast PAP (see below). Canonical PAP in the absence of substrates assumes a much more open conformation (Bard et al., 2000; Martin et al., 2000) and undergoes large conformational changes upon substrate binding (Balbo and Bohm, 2007). In contrast, PAPD1 assumes a mostly closed conformation even in the absence of substrates and may have a smaller conformational change upon substrate binding.

The overall structure of the palm and fingers domains of PAPD1 is also similar to that of the RNA editing TUTase2 (Figures 2C and S3) (Deng et al., 2005) and the minimal TUTase4 (Figures 2D and S3) (Stagno et al., 2007a, 2007b) from *T. brucei*, even though these proteins also share less than 20% sequence identity with PAPD1 (Figure S2). Like PAPD1, these two TUTases do not contain an RBD following the fingers domain.

A Separate Domain in the N-Terminal Region of PAPD1

Unexpectedly, the structure of PAPD1 shows that residues 62–133 in the N-terminal region form a separate domain (Figure 2A) with a backbone fold that is similar to RNP-type RBDs (or RNA recognition motifs, RRMs), including that in canonical PAPs, as indicated by a search through the Protein Data Bank with the program DaliLite (Holm et al., 2008). The sequence conservation among these proteins is very low, 10%–20% amino acid identity. The closest structural homolog is the poly(A) binding protein (PABP) (Deo et al., 1999), with a Z score of 5.5 (Figure 2E). This domain is connected to the rest of PAPD1 by a 40-residue linker (Figure 1B), a segment of which is modeled as poly-alanines in one monomer (Figure 2A), partially stabilized by crystal packing. In the other monomer, this linker is disordered.

Residues 62–133 of PAPD1 form a three-stranded antiparallel β sheet with two α helices on one face, and the β-arm from the other monomer of the PAPD1 dimer adds two more strands, making a five-stranded β sheet for this domain (Figure 2E, see below). Most RBDs contain a four-stranded β sheet with two helices on one face, which roughly match the first four strands of the β sheet and the two helices in PAPD1 (Figure 2E). However, the fourth strand in PAPD1 (from the β-arm of the other monomer) runs parallel to the first strand, while it runs antiparallel to the first strand in the RBDs (Figure 2E). A five-stranded β sheet has been observed in a few of the other RBDs, for example, the RRM2 and RRM3 of polypyrimidine tract binding protein (PTB) (Conte et al., 2000; Oberstrass et al., 2005). However, the fifth strand is located at the other edge of the β sheet in these two RRMs, next to the second strand, and so the domain in PAPD1 is quite different from these RRMs.

While this domain in PAPD1 has structural similarity to an RBD, it is not known whether it can actually bind RNA. In its current conformation in the structure, the domain is positioned about 40 Å from the active site, on the opposite face of the palm domain (Figure 2A), and therefore cannot directly contribute to RNA binding in the active site. Moreover, the open face of the β sheet is generally involved in RNA binding in related domains, such as PABP (Figure 2E) (Deo et al., 1999), U1A (Oubridge et al., 1994),

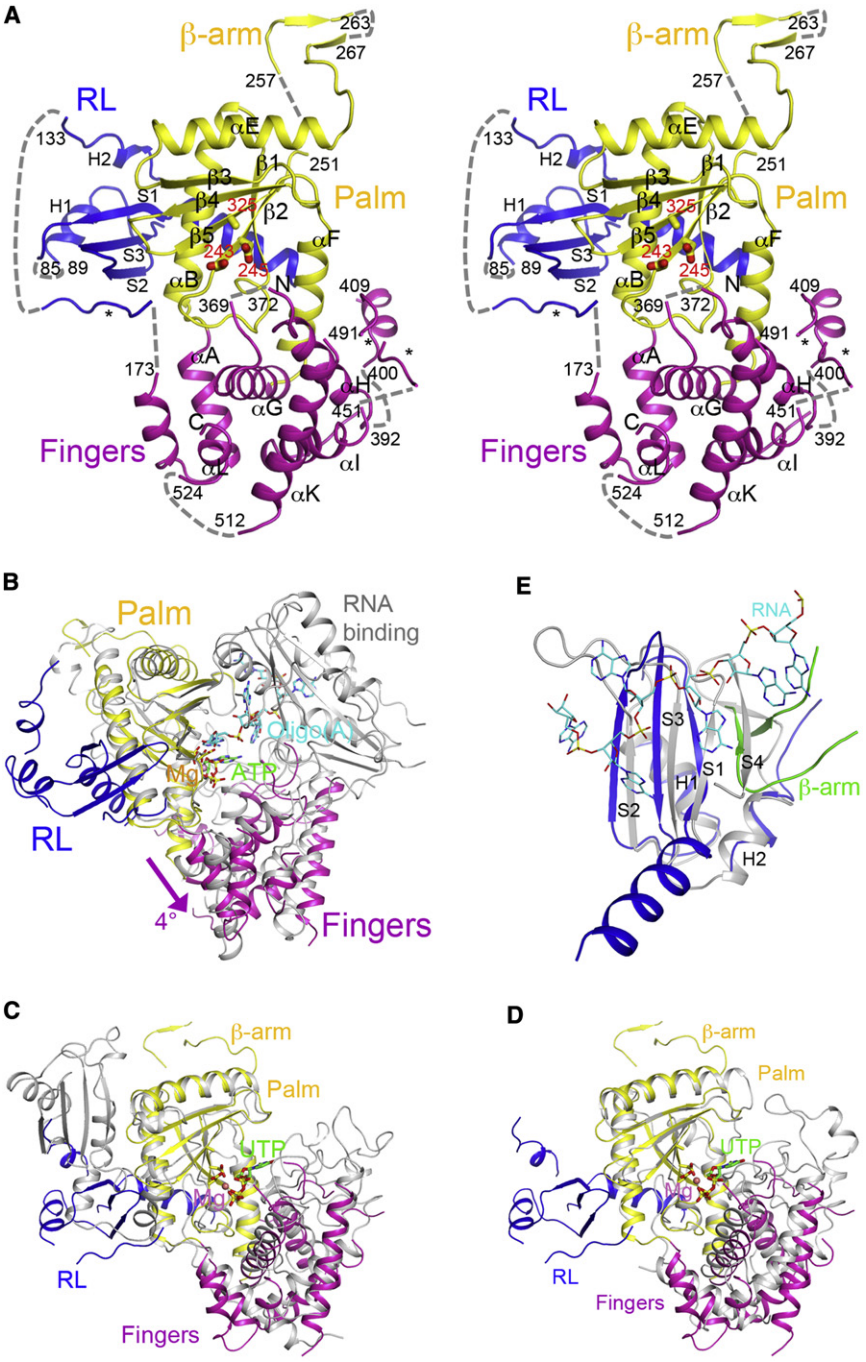

Figure 2. Structure of Human PAPD1 Monomer

(A) Stereo drawing of the structure of human PAPD1 monomer. The two catalytic aspartic acid residues and the D325A mutation in the active site are shown in stick models and labeled in red. Three segments modeled as poly-alanines are indicated with the stars. The missing segments of the structure are indicated with the dashed lines (gray).

(B) Overlay of the structure of human PAPD1 (in color) with that of yeast PAP (in gray) in complex with Mg^{2+} (pink sphere), ATP (green), and oligo (A) (cyan) (Balbo and Bohm, 2007). The fingers domain of PAPD1 is in a slightly more open conformation compared to that in PAP, indicated with the arrow (magenta).

(C) Overlay of the structure of human PAPD1 (in color) and *T. brucei* TUTase2 (in gray) (Deng et al., 2005). The inserted domain in the palm domain of TUTase2 is in a different location compared to the RL domain of PAPD1.

(D) Overlay of the structure of human PAPD1 (in color) and *T. brucei* TUTase4 (in gray) (Stagno et al., 2007a; Stagno et al., 2007b). For stereo versions of (C) and (D), please see Figure S3.

(E) Overlay of the RL domain of human PAPD1 (in blue) with the first RRM of PABP (in gray) in complex with oligo(A) (cyan) (Deo et al., 1999). The β-arm of the second monomer of PAPD1 is shown in green, and it clashes with the fourth strand of the RRM. All the structure figures were produced with PyMOL (http://www.pymol.org). See also Figures S2 and S3.

the AU-rich element binding protein Hrp1 (Pérez-Cañadillas, 2006), and the RRM in CstF-64 (Pérez Cañadillas and Varani, 2003). In PAPD1, however, this face and an extra α helix at the N terminus of the domain are in tight contact with the palm domain (Figure 2A), mediated predominantly by hydrophobic residues. The amino acid sequences of the first and third strands do not contain the RNP1 and RNP2 sequence motifs for RNA binding (Burd and Dreyfuss, 1994; Kielkopf et al., 2004; Query et al., 1989). In yeast PAP, on the other hand, the helices of the domain contribute to binding the oligo (A) RNA, while the open face of the β sheet is not involved in binding (Figure 2B) (Balbo and Bohm, 2007). These helices are exposed to the solvent in PAPD1 (Figure 2A), although they do not have strongly electropositive surface patches that could mediate interactions with the RNA phosphate backbone.

The structural analysis therefore suggests that this separate domain in PAPD1 may be primarily involved in protein-protein interactions rather than substrate binding and catalysis, and we have named it the RL (RBD-like) domain. Similar observations have been made on other RBDs, such as that in the splicing factor U2AF (Kielkopf et al., 2001, 2004) and the 68 kDa subunit of the pre-mRNA 3′ end-processing factor CF-I_m (Brown and Gilmartin, 2003; Dettwiler et al., 2004). Due to the long linker between this domain and the rest of the structure, we cannot exclude the possibility of a large conformational change that could bring this domain close to the active site. However, such a change will disrupt the dimer (see below) as well as expose a large hydrophobic surface patch on the palm domain.

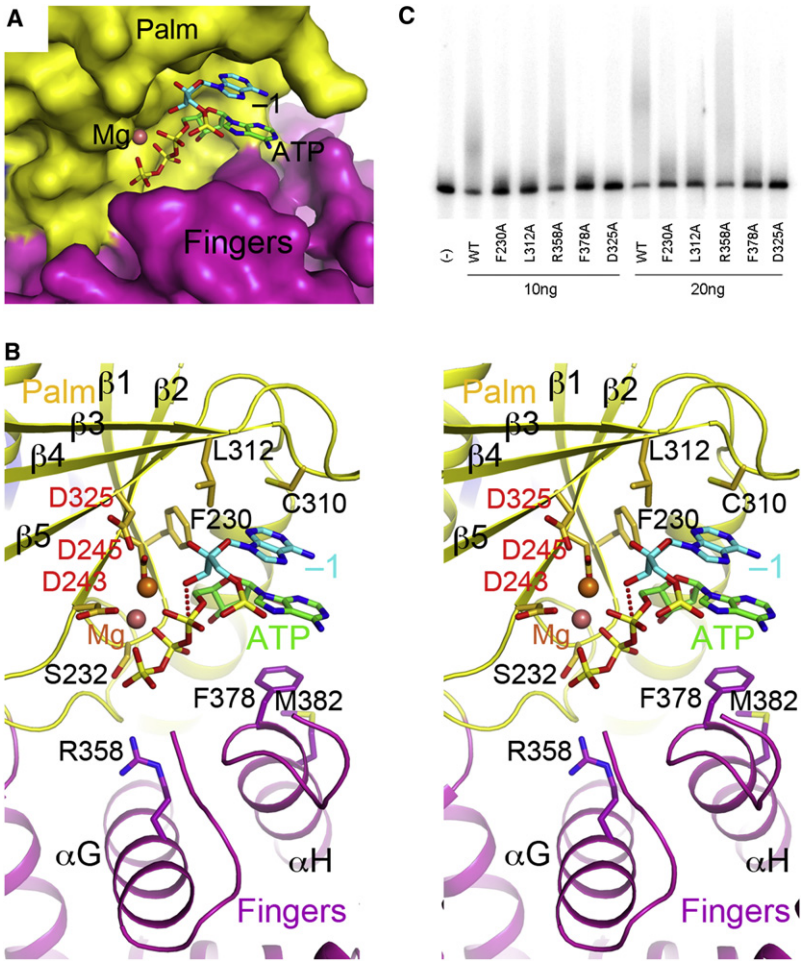

Figure 3. Model of the Active Site of Human PAPD1 with Substrates

(A) Molecular surface of the active site region of PAPD1. The bound positions of Mg^{2+} (pink sphere), ATP (green), and the last nucleotide of the RNA substrate (cyan, labeled −1) are modeled from the structure of yeast PAP (Balbo and Bohm, 2007).

(B) Stereo drawing of the active site model of human PAPD1. Side chains with potentially important roles in catalysis and/or substrate binding are shown as stick models and labeled. The side chain of Asp325 and the two Mg^{2+} ions are modeled. The inline nucleophilic attack of the 3′ hydroxyl group of the last nucleotide of the RNA substrate (the −1 nucleotide) on the α-phosphate of ATP, modeled based on the structure of yeast PAP (Balbo and Bohm, 2007), is indicated by the dashed line in red.

(C) Poly(A) polymerase assays for active site mutants of PAPD1. 10 or 20 ng of each enzyme was used in the assay, and the D325A mutant was included as a control.

In the structure of *T. brucei* TUTase2, the palm domain carries an inserted domain with a backbone fold similar to RBDs, though the function of this domain is not known (Deng et al., 2005). The location of this domain in TUTase2 is different from the RL domain in PAPD1 (Figures 2C and S3).

The Active Site of PAPD1

The active site of PAPD1 is located in a large pocket at the interface between the palm and fingers domains (Figure 3A). As our attempts to obtain the structure of a substrate complex were not successful, we modeled the binding modes of MgATP and the last nucleotide (the −1 nucleotide) of the RNA substrate based on the observations in yeast PAP (Balbo and Bohm, 2007). Both nucleotides can be readily accommodated in the pocket in this model (Figure 3A), suggesting that the active site is formed properly in PAPD1. This is consistent with biochemical studies showing that PAPD1 can carry out catalysis on its own, in the absence of another RNA binding protein (Nagaike et al., 2005). The RBD of yeast PAP interacts with the other nucleotides in the RNA substrate (Figure 2B) and is not involved in the recognition of MgATP and the −1 nucleotide of the RNA (Balbo and Bohm, 2007).

Residues that have important roles in catalysis and/or interactions with the substrates are highly conserved among PAPD1 orthologs (Figure 1B). Many of these residues are also conserved in yeast PAP (Balbo and Bohm, 2007) as well as the *T. brucei* TUTases (Deng et al., 2005; Stagno et al., 2007a, 2007b) (Figure S2). The three catalytic aspartic acid residues in the palm domain coordinate two metal ions and activate the 3′-hydroxyl group of the −1 nucleotide, which is in the correct position for the inline attack on the α-phosphate of ATP to initiate the reaction (Figure 3B). The model suggests that the phosphate groups of ATP may also interact with the main-chain amide and side-chain hydroxyl groups of Ser232 (just after β1 of palm domain) and the side chain of Arg358 (αG of fingers domain). The −1 nucleotide is also located near the side chains of Phe230 and Leu312 (Figure 3B).

The adenine base of ATP is π-stacked with that of the −1 nucleotide (Figure 3B). The other face of this adenine is located near Phe378 (just prior to αH of fingers domain) in the model. It is expected that with a more closed conformation for the fingers domain upon substrate binding, the adenine base of ATP and the phenylalanine side chain could be in π-stacking interactions, as was observed in the TUTases from *T. brucei*, where a tyrosine residue is conserved at this position (Deng et al., 2005; Stagno et al., 2007a, 2007b). Yeast PAP has a valine residue at this position, and its side chain has van der Waals interactions with the adenine base.

To assess the importance of these residues for the catalytic activity of PAPD1, we created the F230A, L312A, R358A, and F378A mutants and characterized their PAP activity. The results of the assays demonstrated that the F230A, L312A, and F378A mutants had greatly reduced PAP activity (Figure 3C), confirming their functional importance and the relevance of our model for the active site of PAPD1. On the other hand, the R358A mutant had little effect on activity, indicating that this side chain is not important for catalysis.

PAPD1 Can Use All Four Nucleotides as Substrates In Vitro

The adenine base of ATP does not appear to be specifically recognized by PAPD1. In the current structure, none of the residues of the enzyme are located within hydrogen-bonding distances of the base. Our in vitro studies in fact suggest that PAPD1 can utilize all four nucleotides as substrates, although it is more active with ATP or UTP (Figure 4A). Therefore, PAPD1 does not have a strict substrate specificity toward the nucleotide, which is consistent with the structural observation. The lowest activity was observed with GTP, and PAPD1 added only a short oligo(G) tail to the RNA in these assays (Figure 4A). The in vitro data are also consistent with observations in vivo on the composition of mitochondrial mRNA tails, which indicated a predominance of A with rare occurrences of G and C (Tomecki et al., 2004).

To characterize further the catalytic activity of PAPD1 toward ATP and UTP, we determined the kinetic parameters for these substrates from a concentration titration (Figure 4B). The reactions followed Michaelis-Menten kinetics, and K_M values for ATP and UTP were calculated to be 0.1 and 0.7 mM, respectively (Figure 4C). The V_{max} values for ATP and UTP were 370 and 310 (arbitrary unit), respectively. Overall, the kinetic analysis suggests that the activity toward ATP is 9-fold higher than UTP (based on V_{max}/K_M values) in this in vitro assay. The reaction contained 20 nM PAPD1 and approximately the same concentration of the RNA substrate.

Studies with the *T. brucei* TUTases suggest that water-mediated hydrogen bonds may be important for substrate selectivity (Stagno et al., 2007a, 2007b). Studies with yeast PAP and other polymerases show that an induced-fit behavior of the enzymes may also be important for substrate selectivity (Balbo and Bohm, 2007; Balbo et al., 2005, 2007; Doublié et al., 1999). On the other hand, PAPD1 appears to have both PAP and TUTase activity (Mullen and Marzluff, 2008; Nagaike et al., 2005; Tomecki et al., 2004) in vivo. It remains to be seen how the enzyme is selective for ATP in the mitochondrion but UTP in the cytoplasm.

A Dimer of PAPD1

The crystal structure of human PAPD1 reveals a dimer, formed by the two molecules in the asymmetric unit (Figure 5A). This is the only tight association among PAPD1 molecules in the crystal. Dimerization of PAPD1 was originally suggested by results from gel filtration chromatography, during purification of the recombinant protein. After determination of the structure, we further confirmed this dimerization using solution light-scattering experiments (Figure S4). This appears to be a unique property of PAPD1, as the canonical PAPs as well as the *T. brucei* TUTases are monomeric in solution. A different nucleotidyl transferase, the *A. fulgidus* tRNA CCA-adding enzyme, is also a dimer (Tomita et al., 2006; Xiong and Steitz, 2004), though it bears no similarity to the dimer of PAPD1. The active site of PAPD1 is located approximately 25 Å from the dimer interface, with no contributions from residues in the other monomer of the dimer (Figure 5A).

The PAPD1 dimer buries approximately 1900 $Å^2$ of the surface area of each monomer, suggesting that the dimer is likely stable,

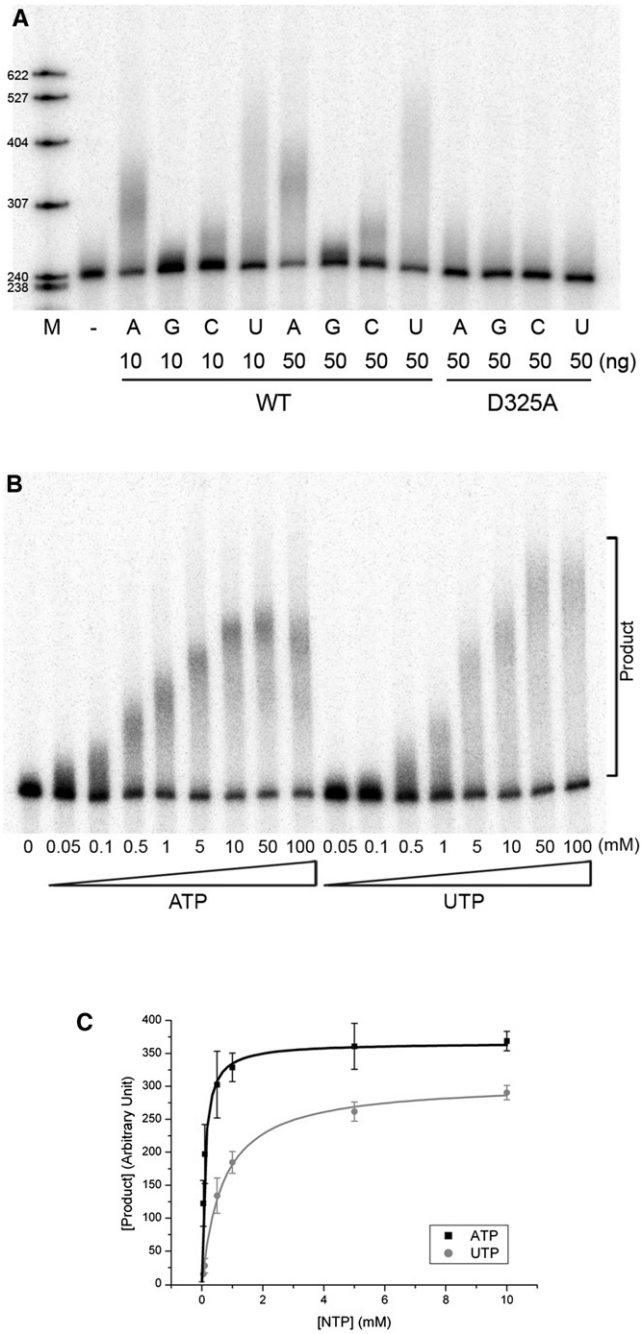

Figure 4. PAPD1 Has Activity toward All Four Nucleotides In Vitro

(A) Catalytic activity of PAPD1 toward the four nucleotides, ATP, GTP, CTP, and UTP. 10 and 50 ng of the wild-type (WT) enzyme were used, and 50 ng of the D325A mutant was also assayed as a control.

(B) Concentration titration of the activity of PAPD1 toward ATP and UTP. The concentrations used for the nucleotides are indicated.

(C) The poly(A) and poly(U) polymerase reaction of PAPD1 follows Michaelis-Menten kinetics. The error bars represent ± 1 SD.

consistent with our studies in solution. Residues in the dimer interface are generally conserved among PAPD1 orthologs (Figure 1B), suggesting that they may also be dimers. The dimer

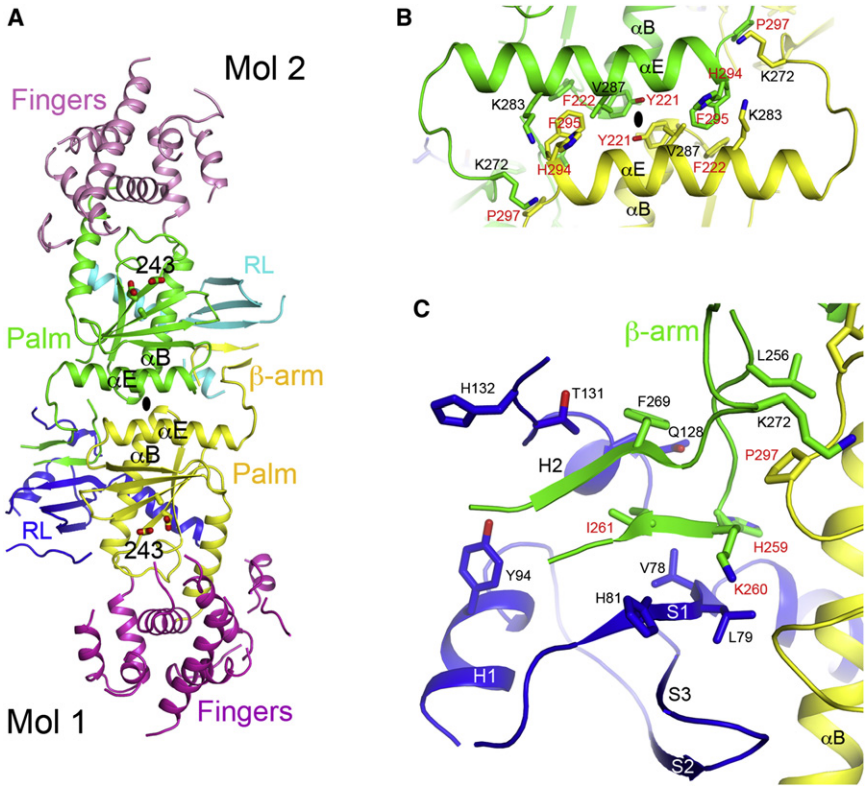

Figure 5. The Dimer of Human PAPD1

(A) Schematic drawing of the human PAPD1 dimer. The domains in the two monomers are given different colors and labeled, and Mol 1 is the one shown in Figure 2A. The catalytic aspartic acid residues in the active sites are shown in stick models. The two-fold axis of the dimer is indicated with the oval in black.

(B) Detailed interactions between helices αE and αB in one contact area of the dimer interface. Residues labeled in red have been selected for mutagenesis experiments.

(C) Detailed interactions between the RL domain of one monomer and the β-arm of the other monomer in the other contact area of the dimer interface. See also Figure S4.

is formed through two major areas of contact between the monomers. In one area, the αE helix in the palm domain of one monomer is located next to its equivalent in the other monomer, and the C-terminal ends of the αB helices of the two monomers are positioned close together as well (Figure 5A). This area of contact consists primarily of van der Waals interactions. Residues His294 (with 80 Å^2 of surface area burial), Phe295 (100 Å^2), and Pro297 (80 Å^2) near the end of helix αE of one monomer are located near residues Lys272 (110 Å^2) and Lys283 (40 Å^2) near the beginning of helix αE and residue Phe222 (20 Å^2) near the end of helix αB of the other monomer (Figure 5B). In addition, residue Tyr221 (60 Å^2) interacts with its symmetry mate across the two-fold axis of the dimer.

In the other area of contact, the β-arm from one monomer is placed next to the RL domain of the other monomer, forming a five-stranded β sheet (Figure 5C). Besides the main-chain hydrogen-bonding interactions in the formation of this larger β sheet, van der Waals interactions for several side chains are also important for this part of the dimer interface. Residues His259 (150 Å^2), Lys260 (100 Å^2), and Ile261 (80 Å^2) in the first strand of the β-arm contribute the most to the buried surface area in this region (Figure 1B).

Dimerization Is Required for PAPD1 Activity

To assess the structural observations on the PAPD1 dimer, we introduced mutations in the interface and characterized their effects on dimerization. Three groups of site-specific mutations, Y221A/F222A (helix αB), H294A/F295A/P297A (αE), and H259A/K260A/I261A (β-arm), were selected based on the structural information. Gel filtration experiments showed that the Y221A/F222A and H294A/F295A/P297A mutants existed in a monomer-dimer equilibrium (data not shown), suggesting that the mutations have destabilized the dimer. In comparison, the H259A/K260A/I261A mutant remained dimeric, consistent with the structural observation that the main-chain atoms of these residues in the β-arm also make important contributions to the dimer interface (Figure 5C).

We next created combinations of the three groups of mutations and found that the H259A/K260A/I261A/H294A/F295A/P297A sextuple mutant, which simultaneously disrupted both areas of contact in the dimer interface, was a stable monomer in solution (Figure 6A), suggesting that the mutation did not disrupt the overall structure of the protein. In comparison, the other combinations produced mutants that were unstable in solution, indicated by the presence of a large amount of aggregates in gel filtration chromatography (data not shown). Similarly, deletion mutants lacking the entire N-terminal RL domain or the β-arm were also found to be unstable in solution. Overall, the mutagenesis experiments confirmed the structural observations and the stability of the PAPD1 dimer.

To assess the functional importance of PAPD1 dimerization, we carried out PAP assays. Wild-type PAPD1 (residues 44–538) showed robust PAP activity in the presence of Mg^{2+} and especially Mn^{2+} cations (Figure 6B). Mutation of one of the conserved aspartic acid residues in the active site, D325A, abolished activity (Figure 6B). Surprisingly, the sextuple mutant, H259A/K260A/I261A/H294A/F295A/P297A, which forms a stable monomer in solution, also failed to show any PAP activity (Figure 6B), indicating that dimerization is essential for PAPD1 function. It is also unlikely that the mutant can have activity toward the UTP substrate.

As the active site of PAPD1 is located far from the dimer interface (Figure 5A), it is not clear why dimerization is required for its PAP activity. One possibility is that dimerization could be important for substrate binding. Electrophoretic mobility shift assays (EMSAs) were not able to detect interactions between wild-type

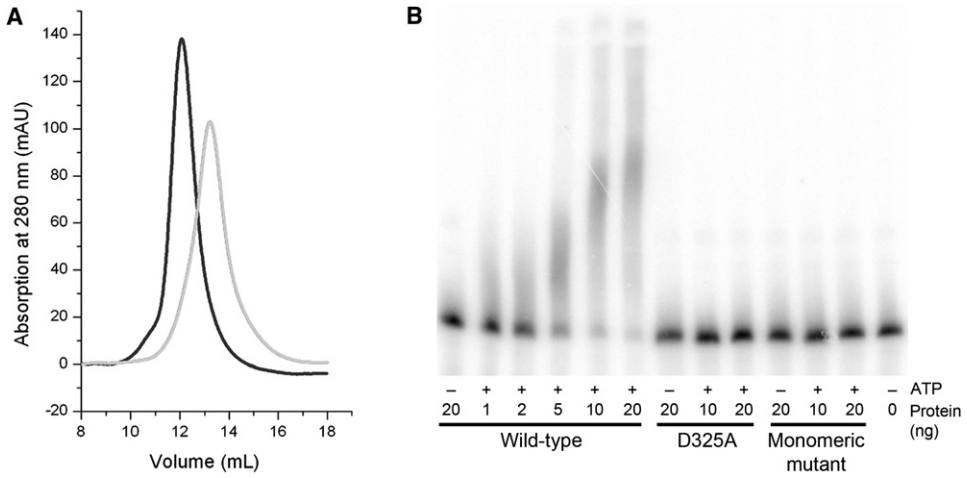

Figure 6. Dimerization Is Required for the Catalytic Activity of PAPD1

(A) Gel filtration data showing that a sextuple mutation in the dimer interface, H259A/K260A/I261A/H294A/F295A/P297A, produces a stable monomer in solution. The profile for wild-type PAPD1 is shown in black and that for the mutant in gray. The void volume on this column is at 7.8 ml, aldolase (158 kDa) at 12.1 ml, and albumin (67 kDa) at 13.4 ml.

(B) Poly(A) polymerase assay for wild-type PAPD1 (residues 44–538), the D325A active site mutant, and the sextuple mutant H259A/K260A/I261A/H294A/F295A/P297A (labeled monomeric mutant).

or monomeric mutant PAPD1 and the RNA substrate at concentrations used in the PAP assay (data not shown). Binding was observed at much higher concentrations of the wild-type and mutant enzymes, but this was probably nonspecific and not catalytically productive. On the other hand, some of the residues in the dimer interface are located in the catalytic palm domain (Figure 5A). Dimerization could indirectly stabilize the conformation of the active site region, while monomers may have detrimental changes in the active site.

In summary, we have produced the structure of a noncanonical PAP, human PAPD1. The structure revealed the enzyme active site as well as a RBD-like (RL) domain in the N-terminal region that contributes to dimerization of the enzyme. Mutagenesis and kinetic studies showed unexpectedly that dimerization is essential for PAP activity. Our observation of a properly formed active site in PAPD1 also has implications for GLD2, Star-PAP, and other noncanonical PAPs. In addition, most of these noncanonical enzymes contain additional sequences in the N-terminal region, prior to the palm and fingers domains. In fact, Star-PAP has an authentic RBD in this region, which is likely involved in RNA binding. Divergent RL domains in this region in the other enzymes could mediate dimerization, as observed for PAPD1, or other protein-protein interactions, for example, recruitment of a separate RNA binding protein.

EXPERIMENTAL PROCEDURES

Protein Expression and Purification

Residues 44–538 of human PAPD1 were subcloned into the pET28a vector (Novagen). The expression construct contained an N-terminal hexa-histidine tag, which was not removed for crystallization. The D325A and other mutants were created with the QuikChange kit (Stratagene). The native protein (wild-type and mutants) was overexpressed overnight in *E. coli* BL21 Rosetta (DE3) cells (Novagen) at 20°C in the presence of 0.5 mM isopropyl-β-D-thiogalactopyranoside (IPTG) (Gold Biotechnology, Inc.). The soluble protein was eluted from nickel affinity beads (QIAGEN) by a buffer containing 50 mM Tris (pH 8.5), 300 mM NaCl, and 250 mM imidazole. The eluted protein was further purified by gel filtration chromatography and then concentrated to 15 mg/ml in a buffer containing 50 mM Tris (pH 8.5), 300 mM NaCl, and 5% (v/v) glycerol. Purified protein samples were flash frozen with liquid nitrogen and then stored at −80°C.

The SeMet protein was produced in *E. coli* BL21 Rosetta (DE3) cells grown in defined M9 media supplemented with selenomethionine and specific amino acids to block endogenous methionine biosynthesis (Doublié et al., 1996). The SeMet protein was purified with the same protocol as the native protein and was concentrated to 35 mg/ml.

The oligomerization state of wild-type PAPD1 was analyzed by size exclusion chromatography followed by static multiangle light-scattering experiments. Gel filtration using a Superose-12 column (GE Healthcare) was also used to analyze the solution behavior of the protein samples.

Protein Crystallization

Crystals of the SeMet D325A mutant were obtained at 20°C by the microbatch method under paraffin oil (Hampton Research; Aliso Viejo, CA). The precipitant solution contained 100 mM MES (pH 6.0), 6% (v/v) PEG4000, 35 mM NaCl, and 5 mM $MgSO_4$. The protein was at 20 mg/ml concentration, and 0.5 mM MgATP was included as an additive. For cryoprotection, the concentration of PEG4000 in the precipitant solution was raised to 30%, and the crystals were flash frozen in liquid nitrogen for diffraction analysis and data collection at 100 K.

Data Collection and Processing

A SeMet multi-wavelength anomalous diffraction (MAD) data set to 3.5 Å resolution and a SeMet single-wavelength anomalous diffraction (SAD) data set to 3.1 Å resolution were collected on an ADSC Quantum4 CCD at the X4A beamline of the National Synchrontron Light Source (NSLS) at Brookhaven National Laboratory. The diffraction images were processed using the HKL package (Otwinowski and Minor, 1997). The crystal belongs to space group $P2_1$, with unit cell parameters of a = 68.7 Å, b = 76.9 Å, c = 87.6 Å, and β = 103.4°. There are two molecules of PAPD1 in the crystallographic asymmetric unit. The data processing statistics are summarized in Table 1 for the SAD data and Table S1 for the MAD data.

Structure Determination and Refinement

The structure of PAPD1 was determined by the MAD method using the anomalous signal of Se (Hendrickson, 1991). Of the 14 expected Se sites in the

asymmetric unit, 12 were located using the program SOLVE, and the reflection phases were calculated and improved with the program SOLVE/RESOLVE (Terwilliger, 2003). The overall figure of merit from the MAD phasing was 0.39 (Table S1). The initial model for one molecule was built with the programs O (Jones et al., 1991) and Coot (Emsley and Cowtan, 2004). The locations of the Se sites, as well as comparison to the structure of yeast PAP (Balbo and Bohm, 2007), guided the tracing of electron density. Residue Met138 is disordered in both monomers, explaining the two missing Se sites. The second molecule in the asymmetric unit was located by molecular replacement using the program COMO (Jogl et al., 2001). The structure refinement was carried out with the programs CNS (Brünger et al., 1998) and Phenix (Adams et al., 2002). We also tried the Refmac refinement program (Murshudov et al., 1997), but could not reduce the R factor further. The statistics on the structure refinement are summarized in Table 1. No solvent molecules were included in the atomic model.

Several segments of the structure were modeled as poly-alanines (Figure 2A), as there was insufficient side-chain electron density for the residues. For the segments in the fingers domain, the location of the residues was guided by the yeast PAP structure (Balbo and Bohm, 2007). For the linker between the N-terminal domain and the palm domain, electron density was recognized in only one of the two molecules (Figure 2A). The average temperature factor value (50 $Å^2$) for these poly-alanine residues was comparable to that for the rest of the protein. If these residues were removed from the atomic model, both the R and free R factor values would increase by 1%.

Polyadenylation Assay

The plasmid used was derived from pG3SVL-A, containing the SV40 late polyadenylation site. Precleaved mRNA substrate uniformly labeled with [α-^{32}P]UTP was prepared by in vitro transcription using SP6 RNA polymerase (Promega) from the plasmid linearized by HpaI (Ryan et al., 2004; Takagaki et al., 1988). Polyadenylation reaction was carried out at 30°C for 30 min. Each reaction contained 1–20 ng of wild-type or D325A mutant protein in 15 μl of reaction buffer, which was composed of ~100 count/second-labeled pre-mRNA substrate, 50 mM Tris (pH 8.0), 40 mM KCl, 1 mM DTT, 0.1 mM ATP, 0.5 mM $MgCl_2$, 0.1 mM $MnCl_2$, and two units of RNase inhibitor (Promega). RNA products were fractionated on 6% polyacrylamide gel in 8.3 M urea and visualized by PhosphorImager.

Electrophoretic Mobility Shift Assay

Various amounts of wild-type and mutant PAPD1 were mixed with body-labeled pre-mRNA substrate (~100 count/second), incubated at room temperature for 15 min, and then fractionated on 6% native polyacrylamide gel. The data were visualized by PhosphorImager.

ACCESSION NUMBERS

The atomic coordinates and structure factors for human PAPD1 have been deposited at the Protein Data Bank with the accession code 3PQ1.

SUPPLEMENTAL INFORMATION

Supplemental Information includes one table, four figures, and Supplemental References and can be found with this article online at doi:10.1016/j.molcel.2011.01.013.

ACKNOWLEDGMENTS

We thank Farhad Forouhar and Jayaraman Seetharaman for help with data collection at the synchrotron source; Randy Abramowitz and John Schwanof for access to the X4A beamline at the NSLS; Dafne Campigli Di Giammartino for help with the polyadenylation assays; and Kehui Xiang, Takashi Nagaike, and Andrew Bohm for helpful discussions. This research is supported in part by grants from the NIH to L.T. (GM077175) and J.L.M. (GM028983).

Received: February 2, 2010
Revised: October 4, 2010
Accepted: December 18, 2010
Published: February 3, 2011

REFERENCES

Adams, P.D., Grosse-Kunstleve, R.W., Hung, L.-W., Ioerger, T.R., McCoy, A.J., Moriarty, N.W., Read, R.J., Sacchettini, J.C., Sauter, N.K., and Terwilliger, T.C. (2002). PHENIX: building new software for automated crystallographic structure determination. Acta Crystallogr. D Biol. Crystallogr. *58*, 1948–1954.

Aravind, L., and Koonin, E.V. (1999). DNA polymerase beta-like nucleotidyltransferase superfamily: identification of three new families, classification and evolutionary history. Nucleic Acids Res. *27*, 1609–1618.

Balbo, P.B., and Bohm, A. (2007). Mechanism of poly(A) polymerase: structure of the enzyme-MgATP-RNA ternary complex and kinetic analysis. Structure *15*, 1117–1131.

Balbo, P.B., Meinke, G., and Bohm, A. (2005). Kinetic studies of yeast polyA polymerase indicate an induced fit mechanism for nucleotide specificity. Biochemistry *44*, 7777–7786.

Balbo, P.B., Toth, J., and Bohm, A. (2007). X-ray crystallographic and steady state fluorescence characterization of the protein dynamics of yeast polyadenylate polymerase. J. Mol. Biol. *366*, 1401–1415.

Bard, J., Zhelkovsky, A.M., Helmling, S., Earnest, T.N., Moore, C.L., and Bohm, A. (2000). Structure of yeast poly(A) polymerase alone and in complex with 3′-dATP. Science *289*, 1346–1349.

Barnard, D.C., Ryan, K., Manley, J.L., and Richter, J.D. (2004). Symplekin and xGLD-2 are required for CPEB-mediated cytoplasmic polyadenylation. Cell *119*, 641–651.

Brown, K.M., and Gilmartin, G.M. (2003). A mechanism for the regulation of pre-mRNA 3′ processing by human cleavage factor Im. Mol. Cell *12*, 1467–1476.

Brünger, A.T., Adams, P.D., Clore, G.M., DeLano, W.L., Gros, P., Grosse-Kunstleve, R.W., Jiang, J.-S., Kuszewski, J., Nilges, M., Pannu, N.S., et al. (1998). Crystallography & NMR system: A new software suite for macromolecular structure determination. Acta Crystallogr. D Biol. Crystallogr. *54*, 905–921.

Burd, C.G., and Dreyfuss, G. (1994). Conserved structures and diversity of functions of RNA-binding proteins. Science *265*, 615–621.

Colgan, D.F., and Manley, J.L. (1997). Mechanism and regulation of mRNA polyadenylation. Genes Dev. *11*, 2755–2766.

Conte, M.R., Grüne, T., Ghuman, J., Kelly, G., Ladas, A., Matthews, S., and Curry, S. (2000). Structure of tandem RNA recognition motifs from polypyrimidine tract binding protein reveals novel features of the RRM fold. EMBO J. *19*, 3132–3141.

Deng, J., Ernst, N.L., Turley, S., Stuart, K.D., and Hol, W.G.J. (2005). Structural basis for UTP specificity of RNA editing TUTases from Trypanosoma brucei. EMBO J. *24*, 4007–4017.

Deo, R.C., Bonanno, J.B., Sonenberg, N., and Burley, S.K. (1999). Recognition of polyadenylate RNA by the poly(A)-binding protein. Cell *98*, 835–845.

Dettwiler, S., Aringhieri, C., Cardinale, S., Keller, W., and Barabino, S.M.L. (2004). Distinct sequence motifs within the 68-kDa subunit of cleavage factor Im mediate RNA binding, protein-protein interactions, and subcellular localization. J. Biol. Chem. *279*, 35788–35797.

Doublié, S., Kapp, U., Aberg, A., Brown, K., Strub, K., and Cusack, S. (1996). Crystallization and preliminary X-ray analysis of the 9 kDa protein of the mouse signal recognition particle and the selenomethionyl-SRP9. FEBS Lett. *384*, 219–221.

Doublié, S., Sawaya, M.R., and Ellenberger, T. (1999). An open and closed case for all polymerases. Structure *7*, R31–R35.

Edmonds, M. (2002). A history of poly A sequences: from formation to factors to function. Prog. Nucleic Acid Res. Mol. Biol. *71*, 285–389.

Emsley, P., and Cowtan, K.D. (2004). Coot: model-building tools for molecular graphics. Acta Crystallogr. D Biol. Crystallogr. *60*, 2126–2132.

Hendrickson, W.A. (1991). Determination of macromolecular structures from anomalous diffraction of synchrotron radiation. Science *254*, 51–58.

Heo, I., Joo, C., Kim, Y.-K., Ha, M., Yoon, M.-J., Cho, J., Yeom, K.-H., Han, J., and Kim, V.N. (2009). TUT4 in concert with Lin28 suppresses microRNA biogenesis through pre-microRNA uridylation. Cell *138*, 696–708.

Holm, L., Kääriäinen, S., Rosenström, P., and Schenkel, A. (2008). Searching protein structure databases with DaliLite v.3. Bioinformatics *24*, 2780–2781.

Jogl, G., Tao, X., Xu, Y., and Tong, L. (2001). COMO: a program for combined molecular replacement. Acta Crystallogr. D Biol. Crystallogr. *57*, 1127–1134.

Jones, T.A., Zou, J.Y., Cowan, S.W., and Kjeldgaard, M. (1991). Improved methods for building protein models in electron density maps and the location of errors in these models. Acta Crystallogr. A *47*, 110–119.

Katoh, T., Sakaguchi, Y., Miyauchi, K., Suzuki, T., Kashiwabara, S.-I., Baba, T., and Suzuki, T. (2009). Selective stabilization of mammalian microRNAs by 3′ adenylation mediated by the cytoplasmic poly(A) polymerase GLD-2. Genes Dev. *23*, 433–438.

Kielkopf, C.L., Rodionova, N.A., Green, M.R., and Burley, S.K. (2001). A novel peptide recognition mode revealed by the X-ray structure of a core U2AF35/U2AF65 heterodimer. Cell *106*, 595–605.

Kielkopf, C.L., Lücke, S., and Green, M.R. (2004). U2AF homology motifs: protein recognition in the RRM world. Genes Dev. *18*, 1513–1526.

Kwak, J.E., and Wickens, M. (2007). A family of poly(U) polymerases. RNA *13*, 860–867.

Kwak, J.E., Wang, L., Ballantyne, S., Kimble, J., and Wickens, M. (2004). Mammalian GLD-2 homologs are poly(A) polymerases. Proc. Natl. Acad. Sci. USA *101*, 4407–4412.

Mandel, C.R., Bai, Y., and Tong, L. (2008). Protein factors in pre-mRNA 3′-end processing. Cell. Mol. Life Sci. *65*, 1099–1122.

Martin, G., and Keller, W. (2007). RNA-specific ribonucleotidyl transferases. RNA *13*, 1834–1849.

Martin, G., Keller, W., and Doublié, S. (2000). Crystal structure of mammalian poly(A) polymerase in complex with an analog of ATP. EMBO J. *19*, 4193–4203.

Martin, G., Möglich, A., Keller, W., and Doublié, S. (2004). Biochemical and structural insights into substrate binding and catalytic mechanism of mammalian poly(A) polymerase. J. Mol. Biol. *341*, 911–925.

Mellman, D.L., Gonzales, M.L., Song, C., Barlow, C.A., Wang, P., Kendziorski, C., and Anderson, R.A. (2008). A PtdIns4,5P2-regulated nuclear poly(A) polymerase controls expression of select mRNAs. Nature *451*, 1013–1017.

Mullen, T.E., and Marzluff, W.F. (2008). Degradation of histone mRNA requires oligouridylation followed by decapping and simultaneous degradation of the mRNA both 5′ to 3′ and 3′ to 5′. Genes Dev. *22*, 50–65.

Murshudov, G.N., Vagin, A.A., and Dodson, E.J. (1997). Refinement of macromolecular structures by the maximum-likelihood method. Acta Crystallogr. D Biol. Crystallogr. *53*, 240–255.

Nagaike, T., Suzuki, T., Katoh, T., and Ueda, T. (2005). Human mitochondrial mRNAs are stabilized with polyadenylation regulated by mitochondria-specific poly(A) polymerase and polynucleotide phosphorylase. J. Biol. Chem. *280*, 19721–19727.

Nagaike, T., Suzuki, T., and Ueda, T. (2008). Polyadenylation in mammalian mitochondria: insights from recent studies. Biochim. Biophys. Acta *1779*, 266–269.

Oberstrass, F.C., Auweter, S.D., Erat, M., Hargous, Y., Henning, A., Wenter, P., Reymond, L., Amir-Ahmady, B., Pitsch, S., Black, D.L., and Allain, F.H. (2005). Structure of PTB bound to RNA: specific binding and implications for splicing regulation. Science *309*, 2054–2057.

Otwinowski, Z., and Minor, W. (1997). Processing of X-ray diffraction data collected in oscillation mode. Methods Enzymol. *276*, 307–326.

Oubridge, C., Ito, N., Evans, P.R., Teo, C.H., and Nagai, K. (1994). Crystal structure at 1.92 A resolution of the RNA-binding domain of the U1A spliceosomal protein complexed with an RNA hairpin. Nature *372*, 432–438.

Pérez-Cañadillas, J.-M. (2006). Grabbing the message: structural basis of mRNA 3′UTR recognition by Hrp1. EMBO J. *25*, 3167–3178.

Pérez Cañadillas, J.M., and Varani, G. (2003). Recognition of GU-rich polyadenylation regulatory elements by human CstF-64 protein. EMBO J. *22*, 2821–2830.

Proudfoot, N.J., and O'Sullivan, J. (2002). Polyadenylation: a tail of two complexes. Curr. Biol. *12*, R855–R857.

Query, C.C., Bentley, R.C., and Keene, J.D. (1989). A common RNA recognition motif identified within a defined U1 RNA binding domain of the 70K U1 snRNP protein. Cell *57*, 89–101.

Rissland, O.S., Mikulasova, A., and Norbury, C.J. (2007). Efficient RNA polyuridylation by noncanonical poly(A) polymerases. Mol. Cell. Biol. *27*, 3612–3624.

Ryan, K., Calvo, O., and Manley, J.L. (2004). Evidence that polyadenylation factor CPSF-73 is the mRNA 3′ processing endonuclease. RNA *10*, 565–573.

Stagno, J., Aphasizheva, I., Aphasizhev, R., and Luecke, H. (2007a). Dual role of the RNA substrate in selectivity and catalysis by terminal uridylyl transferases. Proc. Natl. Acad. Sci. USA *104*, 14634–14639.

Stagno, J., Aphasizheva, I., Rosengarth, A., Luecke, H., and Aphasizhev, R. (2007b). UTP-bound and Apo structures of a minimal RNA uridylyltransferase. J. Mol. Biol. *366*, 882–899.

Stevenson, A.L., and Norbury, C.J. (2006). The Cid1 family of non-canonical poly(A) polymerases. Yeast *23*, 991–1000.

Takagaki, Y., Ryner, L.C., and Manley, J.L. (1988). Separation and characterization of a poly(A) polymerase and a cleavage/specificity factor required for pre-mRNA polyadenylation. Cell *52*, 731–742.

Terwilliger, T.C. (2003). SOLVE and RESOLVE: automated structure solution and density modification. Methods Enzymol. *374*, 22–37.

Tomecki, R., Dmochowska, A., Gewartowski, K., Dziembowski, A., and Stepien, P.P. (2004). Identification of a novel human nuclear-encoded mitochondrial poly(A) polymerase. Nucleic Acids Res. *32*, 6001–6014.

Tomita, K., Ishitani, R., Fukai, S., and Nureki, O. (2006). Complete crystallographic analysis of the dynamics of CCA sequence addition. Nature *443*, 956–960.

Trippe, R., Guschina, E., Hossbach, M., Urlaub, H., Lührmann, R., and Benecke, B.-J. (2006). Identification, cloning, and functional analysis of the human U6 snRNA-specific terminal uridylyl transferase. RNA *12*, 1494–1504.

Vinciguerra, P., and Stutz, F. (2004). mRNA export: an assembly line from genes to nuclear pores. Curr. Opin. Cell Biol. *16*, 285–292.

Wang, L., Eckmann, C.R., Kadyk, L.C., Wickens, M., and Kimble, J. (2002). A regulatory cytoplasmic poly(A) polymerase in Caenorhabditis elegans. Nature *419*, 312–316.

Xiao, Q., Wu, X.-L., Michal, J.J., Reeves, J.J., Busboom, J.R., Thorgaard, G.H., and Jiang, Z. (2006). A novel nuclear-encoded mitochondrial poly(A) polymerase PAPD1 is a potential candidate gene for the extreme obesity related phenotypes in mammals. Int. J. Biol. Sci. *2*, 171–178.

Xiong, Y., and Steitz, T.A. (2004). Mechanism of transfer RNA maturation by CCA-adding enzyme without using an oligonucleotide template. Nature *430*, 640–645.

Zhao, J., Hyman, L., and Moore, C.L. (1999). Formation of mRNA 3′ ends in eukaryotes: mechanism, regulation, and interrelationships with other steps in mRNA synthesis. Microbiol. Mol. Biol. Rev. *63*, 405–445.